

# Quasiparticle states in superconducting superlattices

Mihajlo Vanević<sup>a</sup> and Zoran Radović

Department of Physics, University of Belgrade, P. O. Box 368, 11001 Belgrade, Serbia and Montenegro

Received: April 3, 2019/ Revised version: date

**Abstract.** The energy bands and the global density of states are computed for superconductor / normal-metal superlattices in the clean limit. Dispersion relations are derived for the general case of insulating interfaces, including the mismatch of Fermi velocities and effective band masses. We focus on the influence of finite interface transparency and compare our results with those for transparent superlattices and trilayers. Analogously to the rapid, on the atomic scale, variation of the energy dispersion with layer thicknesses in transparent superlattices, we find strong oscillations of the almost flat energy bands (transmission resonances) in the case of finite transparency. In small-period transparent superlattices, the BCS coherence peak disappears and a similar subgap peak is formed due to the Andreev process. With decreasing interface transparency, the characteristic double peak structure in the global density of states develops towards a gapless BCS-like result in the tunnel limit. This effect can be used as a reliable STM probe for interface transparency.

**PACS.** 74.45.+c Proximity effects; Andreev effect; SN and SNS junctions

## 1 Introduction

The artificial S/N superlattices consisting of alternating superconductor (S) and normal-metal or semiconductor (N) layers have been studied for some time already [1,2,3,4,5,6,7,8], see also [9,10]. The recent advancement of nanofabrication technology and experimental techniques [11], as well as intrinsically layered structure of high- $T_c$  superconductors [12,13,14] has reinvigorated the long standing interest in understanding the effects inherent to clean superconducting heterostructures [15,16,17]. The size and coherence effects have been studied recently for double barrier SNS and NSN junctions in the clean limit based on the solutions of Gor'kov and Bogoliubov–de Gennes (BdG) equations [18,19,20,21,22].

In this paper we extend the previous approach of Tanaka and Tsukada [6] and Plehn et al. [7] to the more general case of superlattices with finite interlayer transparency. We present comprehensive and systematic analysis of the influence of interface transparency on the quasiparticle band structure and density of states for wide range of the superlattice parameters. Due to the phase coherence of electronic wave functions [19,20,21,22] the energy spectrum is gapless in superlattices with thin S layers and transparent interfaces, and splits into almost flat bands (transmission resonances) with decreasing transparency. For thick S layers, the subgap bands are formed due to the Andreev reflection [23] which leads to conversion of

the Cooper pairs in superconducting layers into correlated electrons and holes in the normal layers. Although the calculations are performed in the clean limit, which is appropriate for relatively thin layers, the influence of impurities on the density of states can be taken into account by replacing the superconducting coherence length with an effective one, as shown by Halterman and Valls [24] in comparison with experiments of Moussy et al. [11]. Our results for density of states in superlattices with layer thicknesses smaller than the superconducting correlation length, qualitatively confirm main features previously obtained by Bulaevskii and Zyskin [4] and Buzdin et al. [5] for atomic-scale layered systems within the tight binding approximation.

## 2 The model

The system under consideration is an S/N superlattice in the clean limit, consisting of alternating superconducting and normal-metal (or semiconductor) layers of thickness  $d_S$  and  $d_N$ , with insulating interfaces modelled as thin potential-energy barriers. The superconducting layers are characterized by constant pair potential  $\Delta_0$ , and zero phase difference,  $\phi = 0$ , is assumed across the superlattice. Effective band masses and electrostatic potentials of the two metals are  $m_S$  ( $m_N$ ) and  $U_S$  ( $U_N$ ), respectively. The superlattice is uniform in  $x - y$  planes and the  $z$  axis is perpendicular to the layers.

Quasiparticle propagation in the superlattice is described by the Bogoliubov–de Gennes equation

$$\begin{pmatrix} H_0(\mathbf{r}) & \Delta(\mathbf{r}) \\ \Delta^*(\mathbf{r}) & -H_0^*(\mathbf{r}) \end{pmatrix} \Psi(\mathbf{r}) = E\Psi(\mathbf{r}), \quad (1)$$

<sup>a</sup> *Present address:* Department of Physics, University of Basel, Klingelbergstrasse 82, 4056 Basel, Switzerland; e-mail: mihajlo.vanevic@unibas.ch

where  $\Psi(\mathbf{r}) = (u(\mathbf{r}), v(\mathbf{r}))^T$  is the two-component wave function in the electron-hole Nambu space, the quasiparticle energy  $E$  is measured with respect to the chemical potential  $\mu$ , and the hamiltonian  $H_0$  within the superlattice period  $a = d_N + d_S$ , for  $z \in (-d_N, d_S)$ , is given by

$$H_0(\mathbf{r}) = -\nabla \frac{\hbar^2}{2m(\mathbf{r})} \nabla + \hat{W} [\delta(z) + \delta(z + d_N)] + U(\mathbf{r}) - \mu. \quad (2)$$

The first term is the quasiparticle kinetic energy in the effective mass approximation [15,25], the second term, with  $\hat{W} = \hbar^2 k_{FS} Z / 2m_S$ , describes finite transparency of S-N interfaces modelled as  $\delta$ -function potential barriers, and dimensionless parameter  $Z$  measures the barrier strength. Fermi energies in N and S layers are  $E_{FN} = \hbar^2 k_{FN}^2 / 2m_N = \mu - U_N$  and  $E_{FS} = \hbar^2 k_{FS}^2 / 2m_S = \mu - U_S$ , respectively. We define the corresponding effective chemical potentials as  $\mu_N = \mu_N(k_{\parallel}) = E_{FN} - (\hbar^2 k_{\parallel}^2 / 2m_N)$  and  $\mu_S = \mu_S(k_{\parallel}) = E_{FS} - (\hbar^2 k_{\parallel}^2 / 2m_S)$ , where  $\mathbf{k}_{\parallel}$  is the conserved quasiparticle momentum parallel to the layers.

Solutions of BdG equation,

$$\Psi(\mathbf{r}) = \begin{pmatrix} u(z) \\ v(z) \end{pmatrix} e^{i\mathbf{k}_{\parallel} \cdot \mathbf{r}}, \quad (3)$$

in N and S layers can be written in the form

$$\begin{pmatrix} u(z) \\ v(z) \end{pmatrix}_N = C_1 \sin(k_N^+ z) \begin{pmatrix} 1 \\ 0 \end{pmatrix} + C_2 \cos(k_N^+ z) \begin{pmatrix} 1 \\ 0 \end{pmatrix} + C_3 \sin(k_N^- z) \begin{pmatrix} 0 \\ 1 \end{pmatrix} + C_4 \cos(k_N^- z) \begin{pmatrix} 0 \\ 1 \end{pmatrix} \quad (4)$$

and

$$\begin{pmatrix} u(z) \\ v(z) \end{pmatrix}_S = C_5 \sin(k_S^+ z) \begin{pmatrix} \bar{u} \\ \bar{v} \end{pmatrix} + C_6 \cos(k_S^+ z) \begin{pmatrix} \bar{u} \\ \bar{v} \end{pmatrix} + C_7 \sin(k_S^- z) \begin{pmatrix} \bar{v} \\ \bar{u} \end{pmatrix} + C_8 \cos(k_S^- z) \begin{pmatrix} \bar{v} \\ \bar{u} \end{pmatrix}. \quad (5)$$

Here,  $\Omega = \sqrt{E^2 - \Delta_0^2}$ ,  $k_N^{\pm} = \sqrt{2m_N(\mu_N \pm E)/\hbar^2}$ ,  $k_S^{\pm} = \sqrt{2m_S(\mu_S \pm \Omega)/\hbar^2}$  and the BCS coherence amplitudes are  $\bar{u} = \sqrt{(1 + \Omega/E)/2}$  and  $\bar{v} = \sqrt{(1 - \Omega/E)/2}$ .

Complex coefficients  $C_1$  through  $C_8$  are determined from the boundary conditions at interfaces  $z = 0$  and  $z = -d_N$  inside the primitive cell

$$\begin{pmatrix} u_N(0) \\ v_N(0) \end{pmatrix} = \begin{pmatrix} u_S(0) \\ v_S(0) \end{pmatrix}, \quad (6)$$

$$\frac{1}{m_N} \begin{pmatrix} u'_N(0) \\ v'_N(0) \end{pmatrix} + \frac{k_{FS}}{m_S} Z \begin{pmatrix} u(0) \\ v(0) \end{pmatrix} = \frac{1}{m_S} \begin{pmatrix} u'_S(0) \\ v'_S(0) \end{pmatrix}, \quad (7)$$

$$e^{iKa} \begin{pmatrix} u_N(-d_N) \\ v_N(-d_N) \end{pmatrix} = \begin{pmatrix} u_S(d_S) \\ v_S(d_S) \end{pmatrix}, \quad (8)$$

$$\begin{aligned} \frac{e^{iKa}}{m_N} \begin{pmatrix} u'_N(-d_N) \\ v'_N(-d_N) \end{pmatrix} - \frac{k_{FS}}{m_S} Z e^{iKa} \begin{pmatrix} u_N(-d_N) \\ v_N(-d_N) \end{pmatrix} \\ = \frac{1}{m_S} \begin{pmatrix} u'_S(d_S) \\ v'_S(d_S) \end{pmatrix}. \end{aligned} \quad (9)$$

Here, the Bloch condition  $\Psi(x, y, z + a) = e^{iKa} \Psi(x, y, z)$  is used and the crystal momentum  $K$  is taken within the first Brillouin zone,  $K \in (-\pi/a, \pi/a)$ .

Dispersion relation  $E = E_{n,k_{\parallel}}(K)$  can be written in the following implicit form [7]

$$\begin{aligned} \cos(Ka) &= -\tilde{D}_1/4 \pm \sqrt{(\tilde{D}_1/4)^2 - \tilde{D}_2/4 + 1/2} \\ &\equiv F^{\pm}(E, k_{\parallel}), \end{aligned} \quad (10)$$

where  $\tilde{D}_1$  and  $\tilde{D}_2$  are defined in terms of dimensionless quantities  $E/\Delta_0$ ,  $k_{\parallel}/k_{FS}$ ,  $Z$ ,  $d_N/\xi_0$ ,  $d_S/\xi_0$ ,  $m_N/m_S$ ,  $E_{FN}/E_{FS}$ , and  $\Delta_0/E_{FS}$  (see the Appendix).

Global density of states (for both spin orientations) per unit area of the cross section  $L_x L_y$ , averaged over a primitive cell, is given by

$$\begin{aligned} g(E) &= \frac{1}{L_x L_y} \sum_{\sigma, k_{\parallel}, K} \delta(E - E(k_{\parallel}, K)) \\ &= \frac{1}{\pi} \int dk_{\parallel} k_{\parallel} \sum_{i=+,-} \frac{a}{2\pi} \int dK^i \delta(E - E(k_{\parallel}, K^i)) \\ &= \frac{a}{2\pi^2} \int dk_{\parallel} k_{\parallel} \sum_{i=+,-} \left| \frac{\partial K^i}{\partial E(k_{\parallel}, K^i)} \right|_{E(k_{\parallel}, K^i)=E}, \end{aligned} \quad (11)$$

where  $K^{\pm}(E)$  are the solutions of Eq. (10), and

$$\left| \frac{\partial K^i}{\partial E(k_{\parallel}, K^i)} \right| = \frac{1}{a} \left| \frac{\partial \arccos[F^i(E, k_{\parallel})]}{\partial E} \right|. \quad (12)$$

In accordance with Eq. (10), the integration over  $k_{\parallel}$  [or  $\mu_S = \mu_S(k_{\parallel})$ ] in Eq. (11) is limited to the intervals given by

$$(\tilde{D}_1/4)^2 - \tilde{D}_2/4 + 1/2 \geq 0 \quad (13)$$

and

$$|F^{\pm}(E, k_{\parallel})| \leq 1. \quad (14)$$

In the following,  $g(E)$  is normalized to the normal-state value  $\bar{g} = (m_S d_S k_{FS} + m_N d_N k_{FN}) / \pi^2 \hbar^2$ .

Although  $\Delta(\mathbf{r})$  should be treated self-consistently, we can use the stepwise pair potential as a good approximation [18,21,7]. For S/N superlattices with thin S layers the spatial variation of the pair potential is negligible inside the superconductor, but actual  $\Delta_0$  is smaller than the bulk value [21]. For superlattices with thick S films,  $\Delta_0$  can be set to the bulk value.

### 3 Energy bands and density of states

The dispersion relation, Eq. (10), is solved numerically and the global density of states is calculated from Eq. (11)

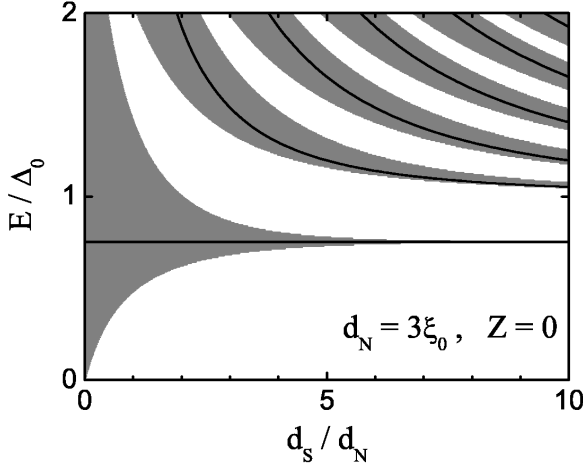


**Fig. 1.** Energy bands as a function of the S layer thickness  $d_S$ , for S/N superlattices with thick N layers,  $d_N = 3\xi_0$ , transparent interfaces,  $Z = 0$ , and  $\mathbf{k}_{||} = 0$ . Andreev bound states ( $E < \Delta_0$ ) and geometrical resonances ( $E > \Delta_0$ ) for the corresponding SNS and NSN trilayers are shown for comparison (solid curves).

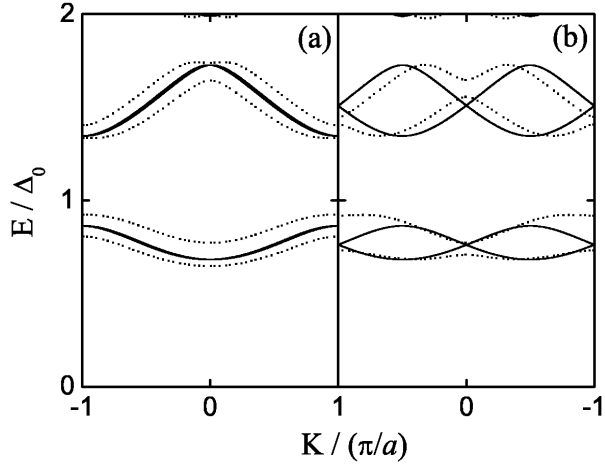


**Fig. 2.** Characteristic dispersion of energy bands illustrated for  $d_N = 3\xi_0$ ,  $Z = 0$ ,  $\mathbf{k}_{||} = 0$ , and (a)  $d_S = 3.0005d_N$ , and (b)  $d_S = 3.0013d_N$ . Bands displayed in (a) are double degenerate for all  $K$ . Dotted curves represent dispersion for finite transparency  $Z = 0.5$ .

for various superlattices and for zero phase difference  $\phi = 0$ . In the following, we focus on the influence of finite interface transparency on quasiparticle band structure and density of states. For simplicity, this is illustrated for equal effective masses and Fermi wave-vectors,  $m_N/m_S = 1$  and  $k_{FN}/k_{FS} = 1$ . Superconductors are characterized by  $\Delta_0/E_{FS} = 10^{-3}$ , which corresponds to the zero-temperature BCS coherence length  $\xi_0 = \hbar^2 k_{FS}/(\pi m_S \Delta_0) \sim 1000\text{\AA}$ .

Energy bands for S/N superlattices with thick N layers, transparent S-N interfaces and quasiparticles propagating perpendicular to the layers ( $\mathbf{k}_{||} = 0$ ) are shown

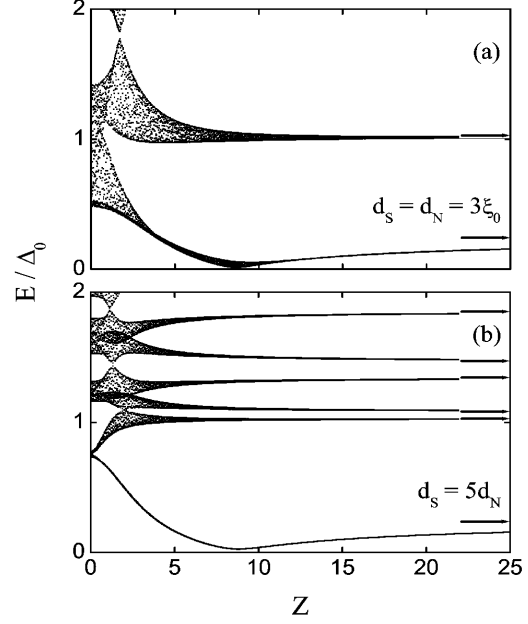


**Fig. 3.** Energy bands as a function of  $Z$ , for  $\mathbf{k}_{||} = 0$  and for two particular S/N superlattices: (a)  $d_S = d_N = 3\xi_0$  and (b)  $d_S = 15\xi_0$ ,  $d_N = 3\xi_0$ . Arrows indicate the bound states in the tunnel limit.

in Fig. 1. Quasicontinuum of energy states corresponding to the crystal momentum within the first Brillouin zone,  $K \in (-\pi/a, \pi/a)$ , is indicated by shading the band width calculated from Eqs. (13) and (14).

For the corresponding SNS trilayer, Andreev bound states,  $E < \Delta_0$ , in the normal interlayer of thickness  $d_N$ , for zero phase difference across the junction, transparent interfaces, and  $\mathbf{k}_{||} = 0$  are given by [26]

$$\frac{E_n}{\Delta_0} = \pi^2 \left[ n + \frac{1}{\pi} \arccos \left( \frac{E_n}{\Delta_0} \right) \right] \frac{1}{d_N/\xi_0}, \quad (15)$$

where  $n = 0, 1, \dots$ . In this case the Andreev bound states are double degenerate. Geometrical resonances,  $E > \Delta_0$ , for the corresponding NSN junction with S interlayer of thickness  $d_S$ , and  $Z = 0$ ,  $\mathbf{k}_{||} = 0$  are given by

$$\frac{E_n}{\Delta_0} = \sqrt{1 + n^2 \frac{\pi^4}{(d_S/\xi_0)^2}}, \quad (16)$$

which follows from the condition  $d_S(k_S^+ - k_S^-) = 2n\pi$ , where  $n = \pm 1, \pm 2, \dots$ . At these energies the Andreev reflection vanishes and the electron is transmitted without creation or annihilation of Cooper pairs [20,21]. Both Andreev bound states and geometrical resonances of the corresponding SNS and NSN trilayers are shown in Fig. 1 for comparison.

In S/N superlattices with thick S layers, the energy band structure above the gap,  $E > \Delta_0$ , is also affected by the Andreev process [16,17]. With increasing  $d_N$ , the band structure dependence on  $d_S/d_N$  remains qualitatively the same as in Fig. 1, with compression and lowering of energy

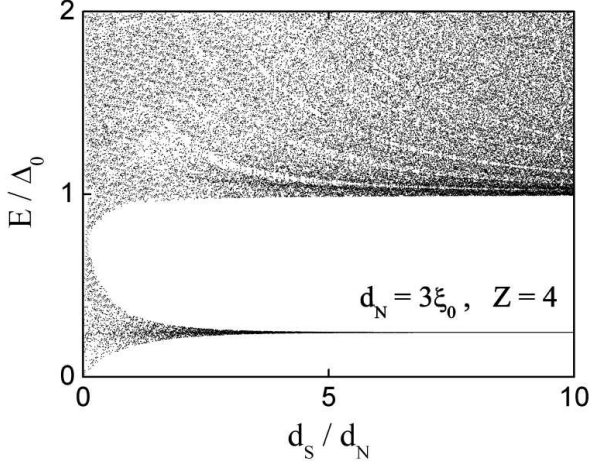


**Fig. 4.** Energy 'bands' for  $d_N = 3\xi_0$ ,  $k_{\parallel} = 0$  and  $Z = 4$ . Shading is produced by the rapid oscillatory dependence of flat energy bands on the S layer thickness.

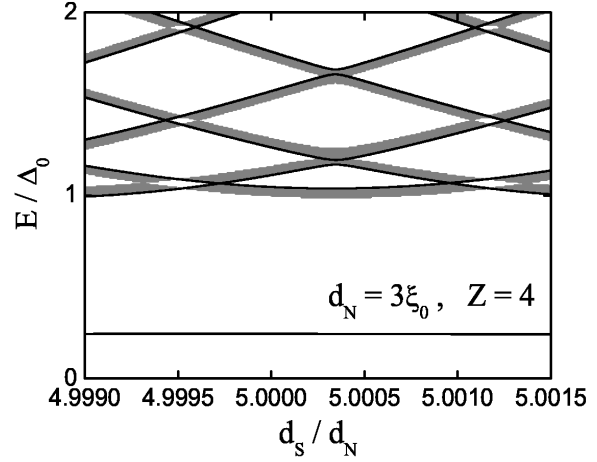


**Fig. 5.** Rapid oscillatory dependence of energy bands on the S layer thickness for nontransparent superlattices. Energy dispersion  $E(K)$  is shown by shading for all  $K$ , solid curves represent  $E(0)$ .

bands that enter the superconducting gap [27]. Although the Andreev reflection is the fundamental mechanism that determines the quasiparticle band structure in S/N superlattices, qualitatively the same results as shown in Fig. 1 are obtained for semiconductor / normal-metal superlattices [28,29]. Characteristic dispersion of energy bands, shown in Fig. 1, is illustrated in Fig. 2 for two close thicknesses of the S layer. For some layer thicknesses the energy bands are double degenerate for all  $K$ , Fig. 2 (a), in contrast with the usual degeneracy at high-symmetry points only (at the center and the ends of the first Brillouin zone), Fig. 2 (b). These two types of dispersion alternate rapidly with the change of layer thicknesses on the atomic scale  $k_F^{-1}$ , while the band width changes on the macroscopic scale.

Finite interface transparency, as well as mismatch of effective masses and Fermi energies [27], lift the degeneracy in  $E(K)$ , Fig. 2, and change the band structure, Fig. 3. For large  $Z$ , energy bands split into pairs of flat bands independent of  $K$ , and there is a significant change of the band energy below the superconducting gap. Approaching the tunnel limit for  $Z \gg 1$ , pairs of adjacent flat energy bands transform into bound states of isolated films defined by  $d_S k_S^{\pm} = n_1 \pi$  and  $d_N k_N^{\pm} = n_2 \pi$ . However, this does not imply that the energy band splitting and decrease of the band widths due to the flattening will be visible in the  $E$  vs.  $d_{S(N)}$  plot (cf. Figs. 1 and 4). Energy levels for  $Z \gg 1$  oscillate rapidly with layer thicknesses on the atomic scale  $k_F^{-1}$ , Fig. 5, so that  $E$  vs.  $d_{S(N)}$  curves fill the energy space quascontinuously on the macroscopic scale, Fig. 4. This implies erasing of the band structure and localization of quasiparticle states in real superlattices with finite interface transparency and slightly unequal layers.

Previous analysis has been made for quasiparticles that propagate perpendicular to the layers. Dependence of energy bands on  $k_{\parallel}$ , i.e. on the effective chemical potential  $\mu_S(k_{\parallel})$ , is illustrated for  $Z = 0$  in Figs. 6 (a) and 7 (a).

Band widths decrease with the increase of  $k_{\parallel}$ , and bands split into pairs of bound states (flat bands) for very large parallel momentum [7], similar to the tunnel limit. The effect of erasing the band structure with finite interface transparency is enhanced with the increase of  $k_{\parallel}$ . Corresponding changes of the global density of states are shown in Figs. 6 (b) and 7 (b). Integration of Eq. (11) is performed over the shaded regions in Figs. 6 (a) and 7 (a), where Eqs. (13) and (14) are satisfied.

Now we shall focus on energy bands and the density of states in thin-layer S/N superlattices, where coherence effects are pronounced and ballistic transport is more likely to take place [21]. Dependence of energy bands on the superlattice period is illustrated in Fig. 8 for  $d_S = d_N$ ,  $k_{\parallel} = 0$ , and for both  $Z = 0$  and  $Z = 1$ . It can be seen that the band structure in transparent thin-layer superlattices differs significantly from the thick-layer case considered in Ref. [7]. For thin layers, dispersion of energy bands is significant, with only a small part of the lower band laying below  $\Delta_0$ . Energy bands as a function of  $k_{\parallel}$ , and for various interface transparencies are shown in Fig. 9. For  $Z = 0$  and  $d_S = d_N$ , the most striking feature is the onset of the lowest energy band at the midgap, practically for any  $k_{\parallel}$ . This is not the case for thick-layer superlattices, where band energy decreases more rapidly down to zero with the increase of  $k_{\parallel}$ , resulting in the left-side "tail" of the subgap peak in the density of states, Figs. 6 and 7. For thin-layer superlattices, finite interface transparency introduces the resonance effect: energy bands penetrate periodically below the midgap with the increase of  $k_{\parallel}$ . This is more pronounced as  $Z$  gets larger, Fig. 9. The corresponding global densities of states for various interface transparencies are shown in Fig. 10.

For transparent interfaces, the density of states is BCS-like with the energy gap  $E_g$  smaller than the pair potential  $\Delta_0$ . The value of  $E_g$  for transparent interfaces, equal ef-

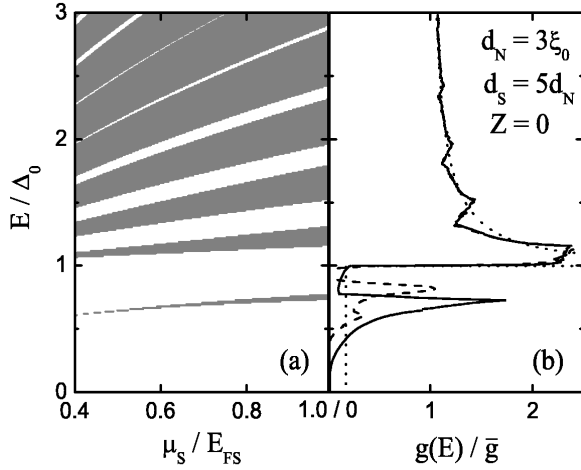


**Fig. 6.** (a) Energy bands as a function of  $\mu_S = \mu_S(k_{\parallel})$ , for S/N superlattice with  $d_S = 15\xi_0$ ,  $d_N = 3\xi_0$  and  $Z = 0$ , and (b) the corresponding global density of states. Global density of states for  $Z = 0.5$  (dashed curve), and in the tunnel limit (dotted curve) are given for comparison.

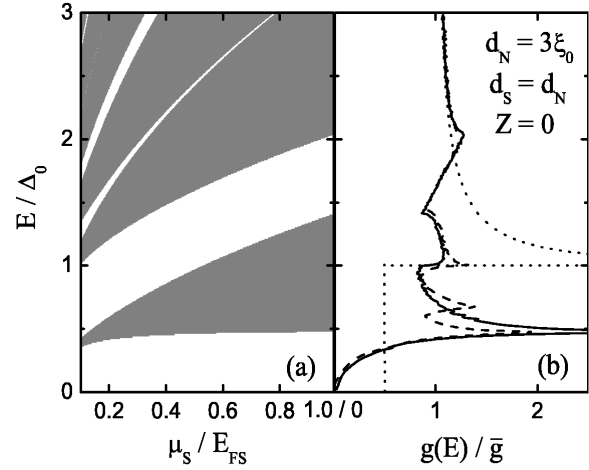


**Fig. 7.** (a) Energy bands as a function of  $\mu_S = \mu_S(k_{\parallel})$ , for S/N superlattice with  $d_S = d_N = 3\xi_0$  and  $Z = 0$ , and (b) the corresponding global density of states. Global density of states for  $Z = 0.5$  (dashed curve), and in the tunnel limit (dotted curve) are given for comparison.

fective masses, and equal Fermi energies can be obtained from the well known dispersion relation [6,30,31]

$$\cos[(K^{\pm} \pm k_{zF})a] = \cos(q\delta d_S) \cos(qd_N) - \delta^{-1} \sin(q\delta d_S) \sin(qd_N), \quad (17)$$

which is a special case of Eq. (10). Here,  $k_{zF} = \sqrt{k_F^2 - k_{\parallel}^2}$ ,  $\delta = \Omega/E$ , and  $q = mE/\hbar^2 k_{zF}$ . For  $d_S, d_N \rightarrow 0$ , from Eqs. (11) and (17) exactly follows [1]

$$E_g = \frac{\Delta_0}{1 + d_N/d_S}. \quad (18)$$

Practically, this simple relation remains valid for the layer thicknesses up to one or two coherence lengths  $\xi_0$ , due to the weak variation of the bottom of the lowest energy band with the layer thickness, Fig. 8 (a).

With decreasing interfacial transparency, the subgap peak in  $g(E)$  at  $E_g$  decays, and the usual BCS coherence peak at  $\Delta_0$  reenters as the superconducting layers become more isolated. In the tunnel limit, the BCS peak at  $\Delta_0$  is completely restored, Fig. 10 (dotted curve in the bottom panel). For thicker layers  $d_S \sim d_N \sim \xi_0$ , the coherence effects are less pronounced and the tunnel limit behavior is practically reached for smaller  $Z \sim 1$ . Previously, this double peak structure in the density of states of S/N superlattices is obtained within the tight binding approximation for atomic-scale layered systems, and apparently observed in high- $T_c$  intrinsically layered superconductors [4,5,13].

## 4 Conclusion

We have derived the dispersion relation for superconductor / normal-metal (semiconductor) superlattices in the

clean limit, generalizing the previous expression of Plehn et al. [7] to include an arbitrary interface transparency and mismatch of effective band masses. The obtained general dispersion relation is used for numerical analysis of the influence of interface transparency on energy band structure and density of states in metallic S/N superlattices. Although we used stepwise approximation for the pair potential, our results will not be altered significantly by the

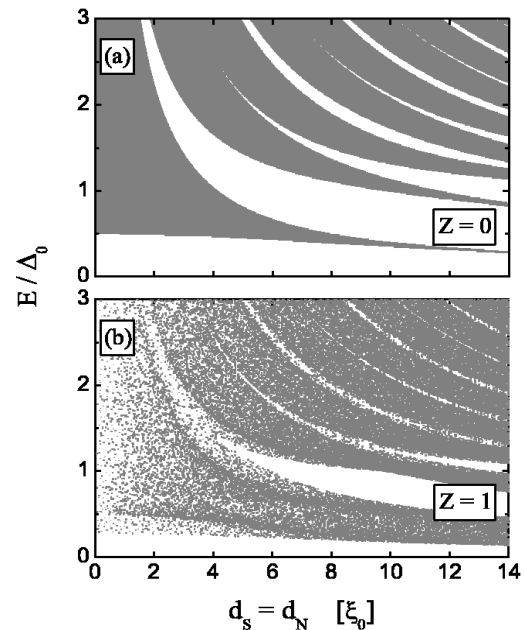


**Fig. 8.** (a) Energy bands for S/N superlattices with  $d_S = d_N$ ,  $k_{\parallel} = 0$  and  $Z = 0$ . (b) Erasing of the band structure with decrease of interface transparency is shown for  $Z = 1$ .

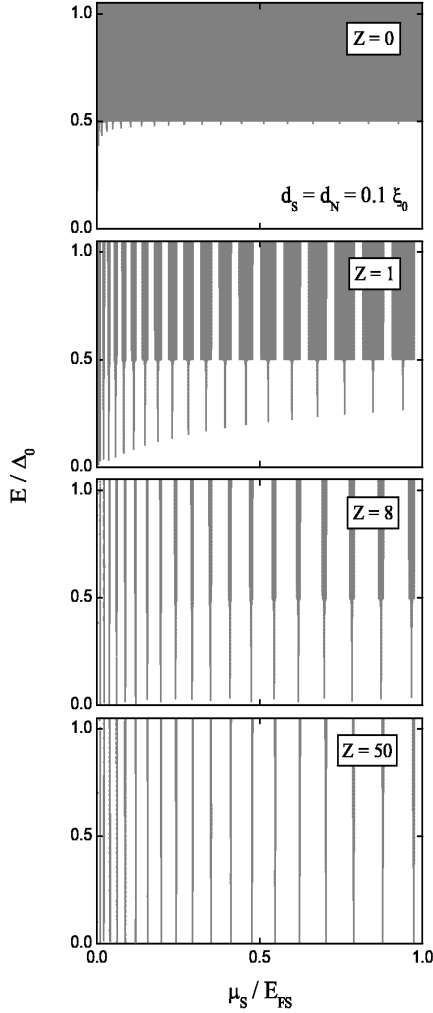


**Fig. 9.** Energy bands as a function of  $\mu_S = \mu_S(k_{||})$ , for S/N superlattice with thin  $d_S = d_N = 0.1\xi_0$  and for various interface transparencies.

fully self-consistent numerical calculations [7], if the actual pair potential (smaller than the bulk value) is taken for thin S layers, and simply the bulk value in the cases of thick S layers, low transparency, and mismatch of Fermi energies or band masses. Our results confirm previously obtained features in the metallic S/N superlattices [6,7], including the limiting cases of double barrier SNS or NSN trilayers [32,17,19,20,21,22], and are in a good qualitative agreement with the results obtained within the tight binding approximation [4,5].

Consequences of the quantum interference effect are strong and rapid (on the atomic scale) geometrical oscillations with layers thickness of the energy dispersion in transparent superlattices, and of the almost flat energy bands (transmission resonances) in the case of finite transparency. Oscillations in the latter case are practically within the band width of the corresponding fully transparent superlattice. Practically, this could imply the localization of quasiparticle states in superlattices with low interface transparency.

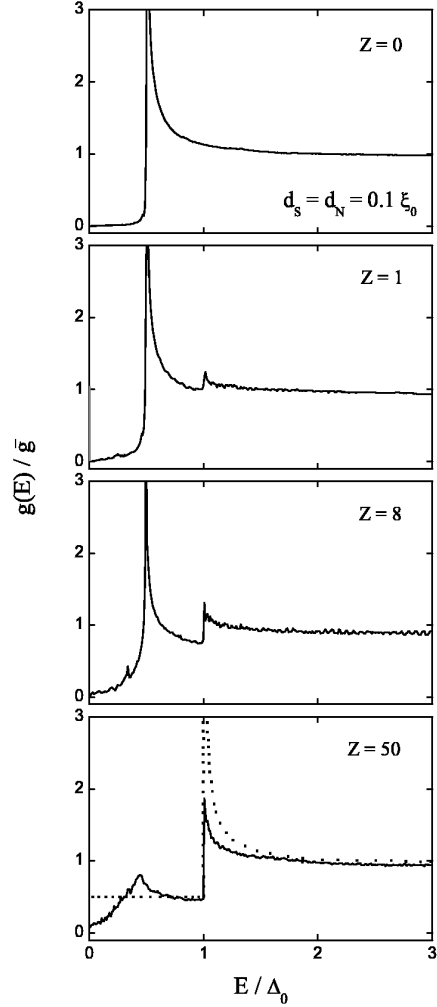


**Fig. 10.** Global density of states for S/N superlattice with thin  $d_S = d_N = 0.1\xi_0$  and for various interface transparencies. Tunnel limit is indicated in the bottom panel (dotted curve). Note that  $\Delta_0$  varies with  $Z$ , being the smallest for  $Z = 0$  (top panel) and reaching the bulk value in the tunnel limit (bottom panel).

Characteristic changes of quasiparticle band structure with decreasing interface transparency are suitably reflected in the global (averaged on the lattice period) density of states, which can be directly measured by STM techniques [13,11]. Oscillations of the density of states are simply related to the band structure for transparent superlattices with thick layers [6]. However, superlattices with the period smaller than the coherence length, when S and N layers lose their individual properties due to strong proximity effect, do not differ significantly from a bulk BCS superconductor, except for a subgap peak in the global density of states instead of the superconductor coherence peak at  $\Delta_0$  [4]. For transparent interfaces, position of the subgap peak is simply related to the lattice parameters. For finite interface transparency, we find the characteristic double peak structure in the global density of states [5]. With decreasing transparency the subgap

peak decreases, only slightly changing the position, while the coherence peak at the gap grows, and the density of states develops towards the gapless BCS result for the bulk superconductor in the tunnel limit. We point out that this double-peak structure of the global density of states in small-period clean-metal S/N superlattices can be used as a reliable experimental probe for interface transparency.

We are grateful to Miloš Božović, Ivana Petković and Boris Grbić for useful discussions. The work has been supported by the Serbian Ministry of Science, Project No. 1899.

## References

1. M.V. Baranov, A.I. Buzdin, L.N. Bulaevskii, Zh. Eksp. Teor. Fiz. **91**, 1063 (1986) [Sov. Phys. JETP **64**, 628 (1986)]
2. S. Takahashi, M. Tachiki, Phys. Rev. B **33**, 4620 (1986); S. Takahashi, M. Tachiki, Phys. Rev. B **34**, 3162 (1986)
3. Z. Radović, M. Ledvij, L. Dobrosavljević-Grujić, Phys. Rev. B **43**, 8613 (1991)
4. L.N. Bulaevskii, M.V. Zyskin, Phys. Rev. B **42**, 10230 (1990)
5. A.I. Buzdin, V.P. Damjanović, A.Yu. Simonov, Physica C **194**, 109 (1992)
6. Yu. Tanaka, M. Tsukada, Phys. Rev. B **44**, 7578 (1991)
7. H. Plehn, O.-J. Wacker, R. Kümmel, Phys. Rev. B **49**, 12140 (1994)
8. S.V. Kuplevakhsky, S.V. Naydenov, A.A. Galiautdinov, Phys. Rev. B **56**, 7858 (1997); S.V. Kuplevakhsky, A.V. Naduev, S.V. Naydenov, Superlatt. Microstruct. **25**, 819 (1999)
9. R. Koperdraad, Ph.D. thesis, Vrije Universiteit Amsterdam, 1995
10. J.B. Ketterson, S.N. Song, *Superconductivity* (Cambridge University Press, 1999)
11. N. Moussy, H. Curtois, B. Pannetier, Europhys. Lett. **55**, 861 (2001); N. Moussy, H. Courtois, B. Pannetier, Rev. Sci. Instrum. **72**, 128 (2001)
12. B.-L. Huang, C.-Yu Mou, Physica C **390**, 167 (2003)
13. L. Buschmann, M. Boekholt, G. Güntherodt, Physica C **203**, 68 (1992)
14. S. Kashiwaya et al., Phys. Rev. B **53**, 2667 (1996)
15. N.A. Mortensen, K. Flensberg, A.-P. Jauho, Phys. Rev. B **59**, 10176 (1999)
16. O. Šipr, B. Györfy, J. Phys. C **8**, 169 (1996)
17. U. Günsenheimer, U. Schüssler, R. Kümmel, Phys. Rev. B **49**, 6111 (1994)
18. Yu. Tanaka, M. Tsukada, Phys. Rev. B **47**, 287 (1993)
19. A. Brinkman, A.A. Golubov, Phys. Rev. B **61**, 11297 (2000)
20. M. Božović, Z. Radović, Phys. Rev. B **66**, 134524 (2002)
21. M. Božović, Z. Pajović, Z. Radović, Physica C **391**, 309 (2003)
22. Z. Radović, N. Lazarides, N. Flytzanis, Phys. Rev. B **68**, 014501 (2003)
23. A.F. Andreev, Pis'ma Zh. Eksp. Teor. Fiz. **46**, 1823 (1964) [JETP Lett. **19**, 1228 (1964)]
24. K. Halterman, O.T. Valls, Phys. Rev. B **66**, 224516 (2002)
25. R.A. Morrow, K.R. Brownstein, Phys. Rev. B **30**, 678 (1984)
26. J. Baselmans, Ph.D. thesis, Rijksuniversiteit Groningen, 2002
27. M. Vanević, Diploma thesis, University of Belgrade, 2003
28. M. Steslicka et al., Surf. Sci. Rep. **47**, 93 (2002)
29. E.L. Ivchenko, G.E. Pikus, *Superlattices and Other Heterostructures – Symmetry and Optical Phenomena*, 2nd edn. (Springer, Berlin, 1997)
30. A.P. van Gelder, Phys. Rev. **181**, 787 (1969)
31. R. Kümmel, Phys. Rev. B **3**, 784 (1971)
32. U. Schüssler, R. Kümmel, Phys. Rev. B **47**, 2754 (1993)

## Appendix

From the boundary conditions, Eqs. (6)–(9), the dispersion relation, Eq. (10), is expressed through  $\tilde{D}_1 = D_1/D_0$  and  $\tilde{D}_2 = D_2/D_0$ , where

$$D_0 = m_r^2 k_N^- k_N^+ k_S^- k_S^+ (\bar{u}^2 - \bar{v}^2)^2, \quad (19)$$

$$D_1 = F_0 + F_1(Zk_{FS}) + F_2(Zk_{FS})^2, \quad (20)$$

$$D_2 = G_0 + G_1(Zk_{FS}) + G_2(Zk_{FS})^2 + G_3(Zk_{FS})^3 + G_4(Zk_{FS})^4. \quad (21)$$

Here,  $m_r = m_N/m_S$ ,  $F_0$  through  $F_2$  and  $G_0$  through  $G_4$  are given by

$$\begin{aligned} F_0 = m_r (\bar{u}^2 - \bar{v}^2) & \left\{ [k_N^+ k_S^+ s_N^- s_S^- (k_N^{-2} + m_r^2 k_S^{-2}) + k_N^- k_S^- s_N^+ s_S^+ (k_N^{+2} + m_r^2 k_S^{+2})] \bar{u}^2 \right. \\ & - [k_N^- k_S^+ s_N^+ s_S^- (k_N^{+2} + m_r^2 k_S^{-2}) + k_N^+ k_S^- s_N^- s_S^+ (k_N^{-2} + m_r^2 k_S^{+2})] \bar{v}^2 \\ & \left. + 2 m_r k_N^- k_N^+ k_S^- k_S^+ [\bar{v}^2 (c_N^+ c_S^- + c_N^- c_S^+) - \bar{u}^2 (c_N^+ c_S^+ + c_N^- c_S^-)] \right\}, \end{aligned} \quad (22)$$

$$\begin{aligned} F_1 = -2 m_r^2 (\bar{u}^2 - \bar{v}^2) & \left\{ k_N^- k_N^+ [k_S^+ s_S^- (c_N^- \bar{u}^2 - c_N^+ \bar{v}^2) + k_S^- s_S^+ (c_N^+ \bar{u}^2 - c_N^- \bar{v}^2)] \right. \\ & \left. + m_r k_S^- k_S^+ [k_N^- s_N^+ (c_S^+ \bar{u}^2 - c_S^- \bar{v}^2) + k_N^+ s_N^- (c_S^- \bar{u}^2 - c_S^+ \bar{v}^2)] \right\}, \end{aligned} \quad (23)$$

$$F_2 = -m_r^3 (\bar{u}^2 - \bar{v}^2) [k_N^- s_N^+ (k_S^- s_S^+ \bar{u}^2 - k_S^+ s_S^- \bar{v}^2) + k_N^+ s_N^- (k_S^+ s_S^- \bar{u}^2 - k_S^- s_S^+ \bar{v}^2)], \quad (24)$$

and

$$\begin{aligned} G_0 = & s_N^- s_N^+ s_S^- s_S^+ (k_N^{-2} k_N^{+2} + m_r^4 k_S^{-2} k_S^{+2}) (\bar{u}^2 - \bar{v}^2)^2 \\ & - 2 (\bar{u}^2 - \bar{v}^2) \left\{ m_r k_N^- k_N^+ [k_N^+ c_N^- s_N^+ (k_S^- c_S^- s_S^+ \bar{u}^2 - k_S^+ c_S^+ s_S^- \bar{v}^2) + k_N^- c_N^+ s_N^- (k_S^+ c_S^+ s_S^- \bar{u}^2 - k_S^- c_S^- s_S^+ \bar{v}^2)] \right. \\ & \left. + m_r^3 k_S^- k_S^+ [k_N^- c_N^- s_N^+ (k_S^+ c_S^- s_S^+ \bar{u}^2 - k_S^- c_S^+ s_S^- \bar{v}^2) + k_N^+ c_N^+ s_N^- (k_S^- c_S^+ s_S^- \bar{u}^2 - k_S^+ c_S^- s_S^+ \bar{v}^2)] \right\} \\ & + m_r^2 \left( 2 k_N^- k_N^+ \{ s_S^- s_S^+ \bar{u}^2 \bar{v}^2 (c_N^- c_N^+ - 1) (k_S^{-2} + k_S^{+2}) \right. \\ & \quad + k_S^- k_S^+ [(1 + 2 c_N^- c_N^+ c_S^- c_S^+) (\bar{u}^4 + \bar{v}^4) - 2 \bar{u}^2 \bar{v}^2 (c_S^- c_S^+ + c_N^- c_N^+ + c_N^- c_N^+ c_S^- c_S^+)] \} \\ & \quad + s_N^- s_N^+ \{ 2 k_S^- k_S^+ \bar{u}^2 \bar{v}^2 (c_S^- c_S^+ - 1) (k_N^{-2} + k_N^{+2}) \\ & \quad \left. + s_S^- s_S^+ [\bar{u}^4 (k_N^{-2} k_S^{+2} + k_N^{+2} k_S^{-2}) + \bar{v}^4 (k_N^{-2} k_S^{-2} + k_N^{+2} k_S^{+2})] \} \right), \end{aligned} \quad (25)$$

$$\begin{aligned} G_1 = & -2 m_r (\bar{u}^2 - \bar{v}^2) \\ & \times \left[ s_N^+ \left( m_r s_N^- \{ c_S^+ k_S^+ s_S^- [k_N^{-2} \bar{u}^2 - k_N^{+2} \bar{v}^2 + m_r^2 k_S^{-2} (\bar{u}^2 - \bar{v}^2)] \right. \right. \\ & \quad \left. \left. + c_S^- k_S^- s_S^+ [k_N^{+2} \bar{u}^2 - k_N^{-2} \bar{v}^2 + m_r^2 k_S^{+2} (\bar{u}^2 - \bar{v}^2)] \right\} \right. \\ & \quad \left. + c_N^- k_N^- \{ -2 c_S^- c_S^+ m_r^2 k_S^- k_S^+ (\bar{u}^2 - \bar{v}^2) + s_S^- s_S^+ [k_N^{+2} (\bar{u}^2 - \bar{v}^2) + m_r^2 (k_S^{+2} \bar{u}^2 - k_S^{-2} \bar{v}^2)] \} \right. \\ & \quad \left. + c_N^+ k_N^+ \left( -2 c_S^- m_r k_S^- (c_S^+ m_r s_N^- k_S^+ + c_N^- k_N^- s_S^+) (\bar{u}^2 - \bar{v}^2) \right. \right. \\ & \quad \left. \left. + s_S^- \{ -2 c_N^- c_S^+ m_r k_N^- k_S^+ (\bar{u}^2 - \bar{v}^2) + s_N^- s_S^+ [k_N^{-2} (\bar{u}^2 - \bar{v}^2) + m_r^2 (k_S^{-2} \bar{u}^2 - k_S^{+2} \bar{v}^2)] \} \right) \right], \end{aligned} \quad (26)$$

$$\begin{aligned} G_2 = & -m_r^2 (\bar{u}^2 - \bar{v}^2) \\ & \times \left( 2 c_S^- m_r k_S^- \{ 2 c_S^+ m_r s_N^- s_N^+ k_S^+ (-\bar{u}^2 + \bar{v}^2) + s_S^+ [-c_N^- k_N^- s_N^+ (\bar{u}^2 - 2 \bar{v}^2) + c_N^+ k_N^+ s_N^- (-2 \bar{u}^2 + \bar{v}^2)] \} \right. \\ & \quad + s_S^- (-2 c_N^+ k_N^+ [c_S^+ m_r s_N^- k_S^+ (\bar{u}^2 - 2 \bar{v}^2) + 2 c_N^- k_N^- s_S^+ (\bar{u}^2 - \bar{v}^2)] \\ & \quad \left. + s_N^+ \{ s_N^- [k_N^{-2} + k_N^{+2} + m_r^2 (k_S^{-2} + k_S^{+2})] s_S^+ (\bar{u}^2 - \bar{v}^2) + 2 c_N^- c_S^+ m_r k_N^- k_S^+ (-2 \bar{u}^2 + \bar{v}^2) \} \right), \end{aligned} \quad (27)$$

$$G_3 = 2 m_r^3 (\bar{u}^2 - \bar{v}^2)^2 \{ m_r k_S^+ s_N^- s_N^+ s_S^- c_S^+ + s_S^+ [k_N^- c_N^- s_N^+ s_S^- + s_N^- (m_r k_S^- c_S^- s_N^+ + k_N^+ c_N^+ s_S^-)] \}, \quad (28)$$



$$G_4 = m_r^4 s_N^- s_N^+ s_S^- s_S^+ (\bar{u}^2 - \bar{v}^2)^2, \quad (29)$$

where  $s_N^\pm \equiv \sin(k_N^\pm d_N)$ ,  $c_N^\pm \equiv \cos(k_N^\pm d_N)$ ,  $s_S^\pm \equiv \sin(k_S^\pm d_S)$ , and  $c_S^\pm \equiv \cos(k_S^\pm d_S)$ . For  $Z = 0$  and  $m_r = 1$  expressions for  $\tilde{D}_1$  and  $\tilde{D}_2$  reduce to the results given in Ref. [7].